

The SMC B-type supergiant AzV322: a g-mode pulsator with a circumstellar disc

R.E. Mennickent^{1*}, Z. Kołaczkowski², I. Soszyński³, M. Cabezas¹, H.E. Garrido⁴

¹Universidad de Concepción, Departamento de Astronomía, Casilla 160-C, Concepción, Chile

²Instytut Astronomiczny Uniwersytetu Wrocławskiego, Kopernika 11, 51-622 Wrocław, Poland

³Warsaw, University Observatory, Al. Ujazdowskie 4, 00-478 Warszawa, Poland

⁴Instituto de Astronomia, Geofísica e Ciências Atmosféricas, Universidade de São Paulo, Rua do Matão 1226, Cidade Universitária, 05508-900 São Paulo, Brazil

ABSTRACT

We present a photometric and spectroscopic study of AzV322, an emission line object located in the Small Magellanic Cloud previously classified between O9 and B0. We analyze 17.5 years of *I* and *V* band OGLE-II, III and IV light curves and find four significant frequencies, viz. $f_1 = 0.386549 \pm 0.000003$, $f_2 = 0.101177 \pm 0.000005$, $f_3 = 0.487726 \pm 0.000015$ and $f_4 = 0.874302 \pm 0.000020$ c/d. The f_1 frequency (period $2^d.58700 \pm 0^d.00002$) provides the stronger periodogram peak and gives a single wave light curve of full amplitude 0.066 mag in the *I*-band. High-resolution optical spectroscopy confirms the early B-type spectral type and reveals prominent double peak Balmer, Paschen, OI 8446 and He I 5875 emissions. The spectral energy distribution shows significant color excess towards long wavelengths possibly attributed to free-free emission in a disk-like envelope. Our analysis yields $T_{eff} = 23\,000 \pm 1500$ K, $\log g = 3.0 \pm 0.5$, $M = 16 \pm 1 M_{\odot}$, $R = 31.0 \pm 1.1 R_{\odot}$, and $L_{bol} = 10^{4.87 \pm 0.06} L_{\odot}$. AzV322 might be a member of the new class of slowly pulsating B supergiants introduced by Saio et al. (2006) and documented by Lefever, Puls, & Aerts (2007), however its circumstellar disk make it an hitherto unique object. Furthermore, we notice that a O-C analysis for f_1 reveals quasi-cyclic changes for the times of maximum in a time scale of 20 years which might indicate a light-travel time effect in a very wide orbit binary with an undetected stellar component.

Key words: stars: early-type, stars: evolution, stars: mass-loss, stars: emission-line, Be, stars: variables: general, supergiants

1 INTRODUCTION

AzV322 (SMC-SC9-161213, SMC113.86165, SMC725.06.36, SMC 2-6, LHA 115-S 36, LIN 406, 2MASS J01025999-7225395, $\alpha_{2000} = 01:02:59.99$, $\delta_{2000} = -72:25:39.1$, B0e, $V = 13.73$ mag, $B - V = 0.00$ mag)¹ is a bright member of the Small Magellanic Cloud classified for the first time as H α emission object by Henize (1956), classification confirmed by Azzopardi, Vigneau, & Macquet (1975) and Meyssonnier & Azzopardi (1993). The star was classified B0 ($V = 13.82$, $B - V = -0.10$, $U - B = -0.95$) based on optical spectra in a list of probable members of the Small Magellanic Cloud (Azzopardi, Vigneau, & Macquet 1975) and photometrically as B0Ib ($V = 13.90$ -, $B - V = -0.11$ -, $U - B = -0.97$ -, $E(B - V) = 0.12$) by Dachs (1970). Later, a classification of O9 II was given based on the analysis of two low-resolution IUE spectra (Smith Neubig & Bruhweiler 1997). The star is included in the group of massive

short-period SMC stars with extra variability by Kourmiotis et al. (2014). A photometric period of $2^d.586981$ is given by these authors based on the analysis of 8-years of OGLE-III data. A finding chart for the star and its surrounding stellar field is shown in Fig. 1.

During our search for interacting binaries with Be-type components in the OGLE-II database, AzV322 was suspected to be a Double Periodic Variable (DPV), i.e. a semidetached Algol-like binary with a long photometric cycle lasting roughly 33 times the orbital period (eg. Mennickent et al. 2003; Mennickent, Otero, & Kołaczkowski 2016; Mennickent 2017). This, and the fact that the star was the brightest of the SMC DPV candidates, motivated the spectroscopic monitoring reported in this paper. However, the DPV classification turned to be spurious since the long period was limited to the time baseline of the OGLE-II database, but not present when considering new photometric time series with longer time baselines. In addition, the first spectra we got showed well developed double emission lines which are unusual for an early B-type supergiant but typical of a classical Be star. All these results pointed to a complex picture which is explored further in the present work.

* E-mail: rmennick@astroudec.cl

¹ <http://simbad.u-strasbg.fr/simbad/>

Let’s remember that classical Be stars are rapidly rotating non-supergiants B-type stars that show or have shown Balmer line emission in the past (Rivinius, Carciofi, & Martayan 2013). The emission is formed in a circumstellar disk by ionization and subsequent recombination of the circumstellar material, mostly neutral hydrogen. The origin of the Be star phenomenon has remained elusive for more than a century, but recent research based on high signal to noise photometry performed with satellites suggests that it is linked to the presence in the stellar surface, of gravity-mode oscillations producing difference frequencies with larger amplitudes than the original ones (Baade et al. 2016). According to these authors, “... *significant dissipation of pulsational energy in the atmosphere may be a cause of mass ejections from Be stars*”. These non-periodic mass ejections, documented in many multi-wavelength studies, are the origin of the circumstellar disk-like envelope characterizing classical Be stars. In spite of these promising advances, more investigation is needed to clarify how Be stars eject mass into the circumstellar medium.

On the other hand, recent evidence for gravity-mode oscillations driven by opacity was also reported in a sample of periodically variable B-type *supergiants*, where the cause for non-vanishing g-mode pulsations, which were expected in principle to be damped, has been attributed to its reflection in the hydrogen-burning shell, which significantly reduces radiative damping in the core (Lefever, Puls, & Aerts 2007; Saio et al. 2006). On the contrary to Be stars, B-type supergiants do not show evidence for a circumstellar disk, but they show P-Cygni type $H\alpha$ emission revealing line formation in an expanding atmosphere, a radiatively driven wind.

In this paper we report pulsations in the B-type supergiant AzV322, which in principle can be attributed to gravitationally-supported oscillation modes. We will show that, in spite of its supergiant classification, AzV322 has attributes of classical Be stars: double peak emission revealing a disk-like envelope and infrared excess compatible with free-free emission in the disk. The study of AzV322 might be relevant in the context of pulsations in hot supergiants and the origin of the Be star phenomenon.

The paper is organized as follow: in Section 2 we introduce the photometric datasets used in our analysis, details of our spectroscopic observations are given in Section 3, in Section 4 we present our results including the light curve analysis, the study of the spectroscopic data and the spectral energy distribution, in Section 5 a discussion is provided along with a possible interpretation for the system and finally our conclusions are given in Section 6.

2 PHOTOMETRIC DATA

The photometric time-series analysed in this paper are taken from the OGLE project databases. We include OGLE-II data (Szymanski 2005)² and OGLE-III/IV data³. The OGLE-IV project is described by Udalski, Szymański, & Szymański (2015). The whole dataset consists of 1529 *I*-band magnitudes and 161 *V*-band magnitudes taken during a time interval of 17.5 years. A summary and characterization of these datasets is given in Table 1.

When studying the spectral energy distribution, we included broad-band photometry extracted from different sources with the aid of the VizieR photometric tool⁴. A compilation of these fluxes and magnitudes is given in Table 2. In the table, when multiple



Figure 1. The stellar field around AzV322 spanning a field of view of 11.5 x 11.5 squared arc minutes; the image, from ESO-MAMA, has a resolution of 0.67 arcsec/pix. AzV322 is shown by a circle at the center of the image. Two open clusters are at the north-west location, OGLE 233 and OGLE 234.

Table 1. Summary of survey photometric observations. The number of measurements, starting and ending times for the series and average magnitude and standard deviation (in magnitudes) are given. Single point uncertainties in the *I*-band and *V*-band are between 4 and 6 mmag.

Database	N	HJD_{start}	HJD_{end}	mag	std.	band
OGLE-II	326	621.86357	1873.69863	13.70	0.03	<i>I</i>
OGLE-III	724	2104.88015	4953.92420	13.71	0.04	<i>I</i>
OGLE-IV	479	5346.93180	7312.65138	13.77	0.03	<i>I</i>
OGLE-II	33	665.92289	1510.59748	13.82	0.03	<i>V</i>
OGLE-III	94	3326.61986	4954.92914	13.81	0.04	<i>V</i>
OGLE-IV	34	5399.87964	6601.58580	13.88	0.04	<i>V</i>

fluxes were present in a given filter, we list the measurement with less error and closer to the documented stellar position.

3 SPECTROSCOPIC DATA

Spectra were taken between November 2006 and August 2009 with the echelle spectrograph mounted at the Irénée du Pont 2.5m telescope⁵ and the *Magellan Inamori Kyocera Echelle* (MIKE⁶) mounted in the 6.5m Clay telescope in Las Campanas Observatory. The du Pont spectra have a wavelength range of 3940–7490 Å and resolving power 40 000. The MIKE double echelle spectrograph provided wavelength coverage of 3390–4965 Å (blue camera) and 4974–9407 Å (red camera) with resolving power also of 40 000. The spectra were reduced and calibrated with IRAF (Tody 1993). The result of this process was a set of continuum-normalized wavelength-calibrated, one-dimensional not flux-calibrated spectra. A summary of these observations is given in Table 3.

² <http://ogledb.astrouw.edu.pl/~ogle/photdb/>

³ OGLE-III/IV data kindly provided by the OGLE team.

⁴ <http://vizier.u-strasbg.fr/vizier/sed/doc/>

⁵ <http://www.lco.cl/telescopes-information/magellan/telescopes-information/irenee-du-pont/instruments/>

⁶ <http://www.lco.cl/telescopes-information/magellan/instruments/mike>

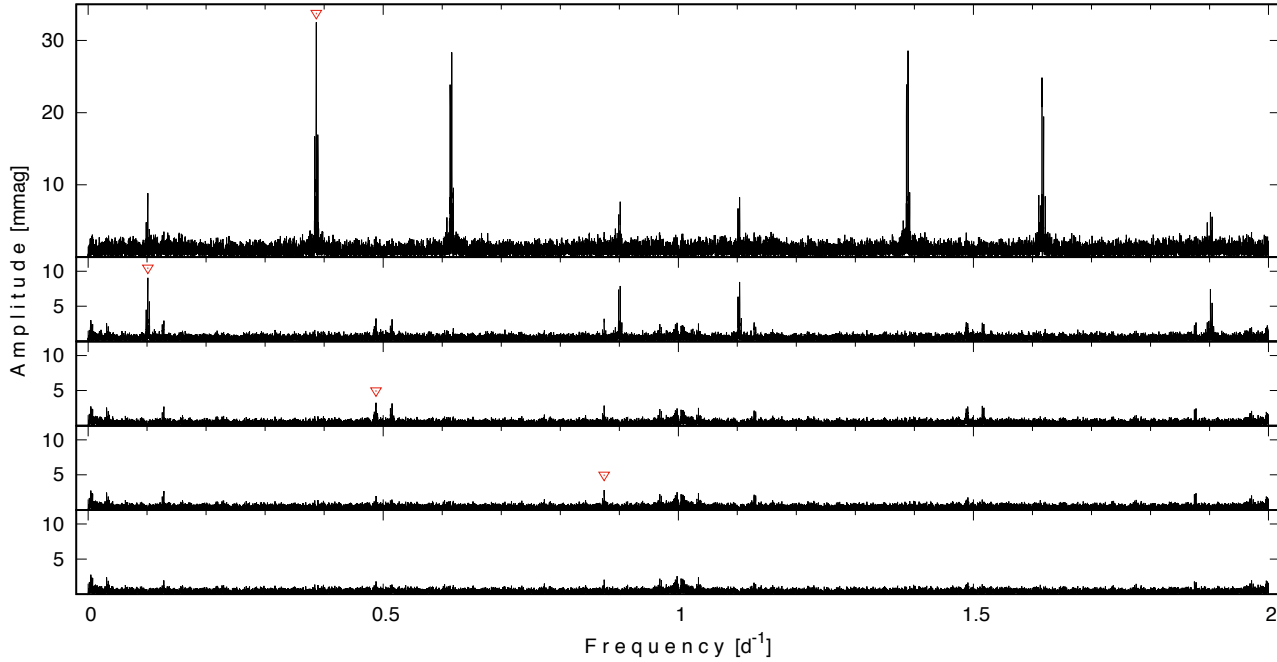


Figure 2. The periodograms showing the whitening process. From up to down the triangles show the frequencies f_1 to f_4 .

Table 2. Fluxes and their errors derived from magnitudes reported by the VizieR photometric tool.

Filter	λ (μm)	f_λ (Jy)	σf_λ (Jy)
Johnson <i>U</i>	3.53E-1	15.2E-3	0.4E-3
Johnson <i>B</i>	4.44E-1	13.7E-3	1.2E-3
Johnson <i>V</i>	5.54E-1	11.7E-3	0.8E-3
Johnson <i>J</i>	1.25E+0	5.57E-3	0.09E-3
Johnson <i>H</i>	1.63E+0	3.96E-3	0.11E-3
Johnson <i>K</i>	2.19E+0	3.45E-3	0.11E-3
Cousins <i>I</i>	7.89E-1	9.09E-3	0.80E-3
DENIS <i>I</i>	7.90E-1	8.91E-3	0.79E-3
SDSS <i>I</i>	7.63E-1	7.78E-3	0.34E-3
SDSS <i>r</i>	6.25E-1	9.27E-3	0.45E-3
SDSS <i>g</i>	4.82E-1	11.3E-3	0.5E-3
2MASS <i>J</i>	1.24E+0	5.33E-3	0.13E-3
2MASS <i>H</i>	1.65E+0	4.20E-3	0.11E-3
2MASS <i>K_s</i>	2.16E+0	3.57E-3	0.11E-3
WISE <i>W1</i>	3.35E+0	1.86E-3	0.04E-3
WISE <i>W2</i>	4.60E+0	1.29E-3	0.03E-3
WISE <i>W3</i>	1.16E+1	5.81E-3	79E-6
WISE <i>W4</i>	2.21E+1	6.10E-3	0.73E-3
IRAC 1	3.55E+0	1.79E-3	0.04E-3
IRAC 2	4.49E+0	1.48E-3	0.02E-3
IRAC 3	5.73E+0	1.10E-3	0.03E-3
IRAC 4	7.87E+0	763.0E-6	37.0E-6

4 RESULTS

4.1 Analysis of the light curve

We removed the long-term tendency in the *I*-band subtracting from the data a spline-function. Since the *V*-band light curve consisted

Table 3. Summary of spectroscopic observations. The heliocentric julian day (HJD - 245 0000) at mid-exposure is given. The *S/N* ratio is calculated in the continuum around 4000 Å. Φ refers to the phase according to the 9^d8837 period calculated according to the ephemerides given in Eq. 1.

Instrument	UT-date	exptime (s)	<i>S/N</i>	HJD	Φ
MIKE	2006-09-26	360	35	4004.70866	0.672
MIKE	2006-10-02	600	40	4010.69670	0.279
MIKE	2006-11-26	300	15	4065.69103	0.847
MIKE	2007-07-20	1110	30	4301.63093	0.738
MIKE	2007-11-08	6300	45	4412.52745	0.967
MIKE	2007-11-09	1000	30	4413.51920	0.068
MIKE	2008-01-05	600	40	4470.51848	0.839
echelle	2009-08-25	2000	15	5068.80851	0.422
echelle	2009-08-25	2000	15	5068.83272	0.424

of much less datapoints, it was corrected shifting the OGLE-II and OGLE-IV data to the average of the OGLE-III dataset. We investigated the resulting *I*-band light curve performing a Fourier analysis with the Period04⁷ software (Lenz & Breger 2005) between 0 and 2 c/d. A dominant frequency $f_1 = 0.386549$ is found in the periodogram, and a subsequent whitening process reveals three additional statistically significant periodic signals, viz. $f_2 = 0.101177$, $f_3 = 0.487726$ and $f_4 = 0.874302$ (Figs. 2, 3 and 4). After the process of subtraction of the four frequencies the residual light curve only shows a bunch of very low frequencies and their aliases around 1 c/d. This is typical for objects with an irregular (erratic) variability at the level of 0.0025 mag. The results of this process are given in Table 4.

Considering the whole dataset, we find the following ephemerides for the maximum of the short-cycle:

⁷ <https://www.univie.ac.at/tops/Period04/>

Table 4. Results of the Fourier analysis of the I -band light curve. Frequencies, amplitudes (average in the case of f_1) and their errors are given.

Label	frequency (d^{-1})	period (d)	amplitude (mag)
f_1	0.386549 ± 0.000003	2.5870	0.0331 ± 0.0006
f_2	0.101177 ± 0.000005	9.8837	0.0095 ± 0.0006
f_3	0.487726 ± 0.000015	2.0503	0.0034 ± 0.0006
f_4	0.874302 ± 0.000020	1.1438	0.0027 ± 0.0007

$$HJD = 2454620.3747(55) + 2^d 587000(17) E \quad (1)$$

Since the dominant frequency f_1 has small side-peaks, likely indicating disturbances in the periodic process (changes of period, amplitude or another parameters), we divided the light curve in seasons for further analysis, which is possible due to the fact that the OGLE project observes the SMC in longer than half year seasons. The time series data with removed signal of f_2 were divided to one-season time-series. For each season we did the fit with fixed frequency f_1 (obtained from the non-linear fit to whole data set), but for every season we estimated amplitude and time of maximum (phase). With these results we can obtain the O-C diagram and see how much the amplitude of f_1 is variable; it shows substantial changes over a long time scale (Fig. 5). Furthermore, the times of maximum change quasi-cyclically in a time scale of 20 years, a scale comparable with the data time baseline (Fig. 6). We notice that the maximum deviations in the O-C diagram are +0.08 and -0.1 cycles or +0.21 and -0.26 days. We did the same analysis for f_2 and find that the amplitude of f_2 is too small and the O-C diagram is too noisy; the points are distributed inside 2σ therefore we considered the variability not significant (Fig. 7). Subsequent frequencies f_3 and f_4 produce light curves of lower amplitude hence no significant result can be obtained with the above analysis for these frequencies.

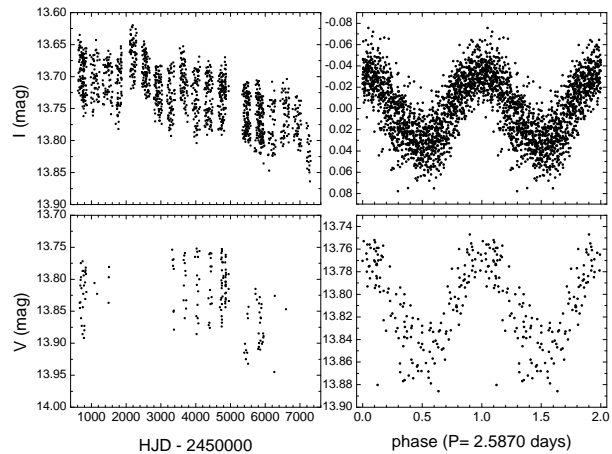
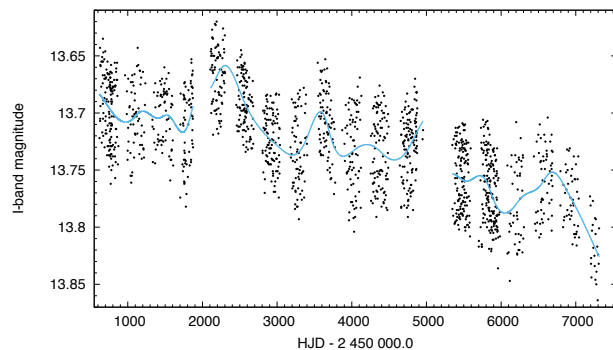
To test if the above results were sensible to the method used for removing the long-term tendencies we performed several tests with different methods and parameters of long-term variability subtraction, for instance we used spline fits for each season separately (and with careful inspection on all steps). We confirm that the results are basically the same. Sometimes we observe additional low-amplitude frequencies, but f_1 , f_2 , f_3 and f_4 are always present in the Fourier analysis (i.e. they are real), and they have always similar (and variable for f_1 and f_2) amplitudes. We conclude that our light-curve analysis is robust and the results reliable.

In the rest of the paper we refer to f_1 as the short-cycle and f_2 as the long-cycle frequency. We notice that the amplitude of the short cycle is larger in the V -band (0.043 mag, estimated from the light curve) than in the I -band (0.033 mag, Table 4).

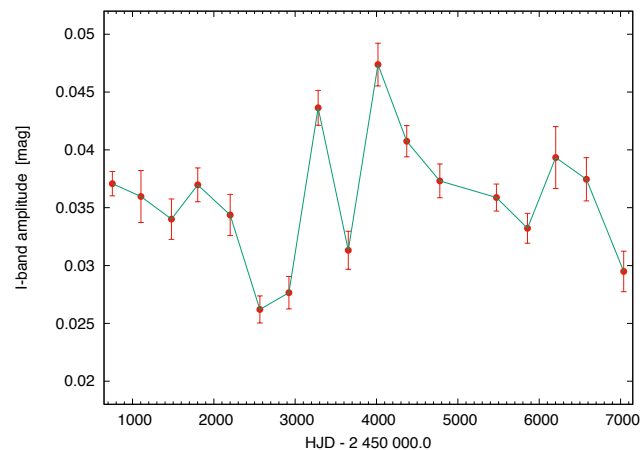
4.2 Analysis of spectroscopic data

The O-type published in the literature is discarded since we do not find He II lines in our spectra. We don't observe either any forbidden emission line so the object is not a B[e] star. MgII 4481 is very weak compared to HeI 4471 indicating an early B-type star. Looking in the line strength ratios HeI 4009/4026 and HeI 4121/4142 we estimate a spectral type B1, according to a comparison with the Gray spectral atlas⁸.

⁸ <https://ned.ipac.caltech.edu/level5/Gray/frames.html>

**Figure 3.** OGLE I -band and V -band light curves spanning 17.5 years (left) and the fit residuals phased with the short period of $2^d 5870$ (right).**Figure 4.** The OGLE I -band light curve and the spline-function used to remove the long-term tendency.

Average properties for the emission lines are presented in Table 5, including the ratio between the violet and red peak intensity relative to the normalized continuum $V/R \equiv (I_V - 1)/(I_R - 1)$. We observe that the equivalent width of the $H\alpha$, $H\beta$ and $H\gamma$ emission lines remains almost constant and only small line profile variability is detected (Fig. 8). The blue emission peak has practically the same intensity that the red emission peak and the peak separation increases with the Balmer series order. This gradient is typical signature of a Keplerian Be star disk. We also observe in the near-infrared the

**Figure 5.** The seasonal amplitudes of the f_1 signal.

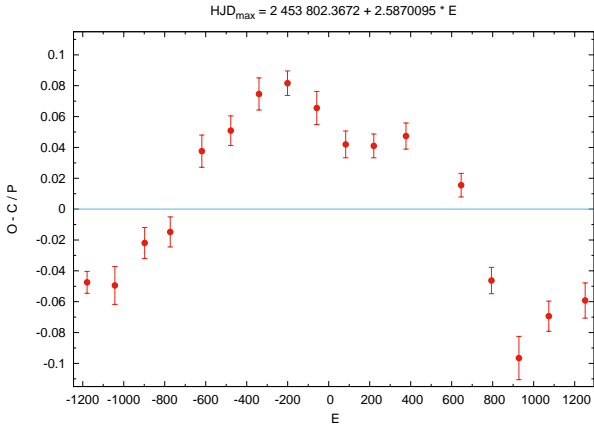


Figure 6. The observed minus calculated diagram for f_1 .

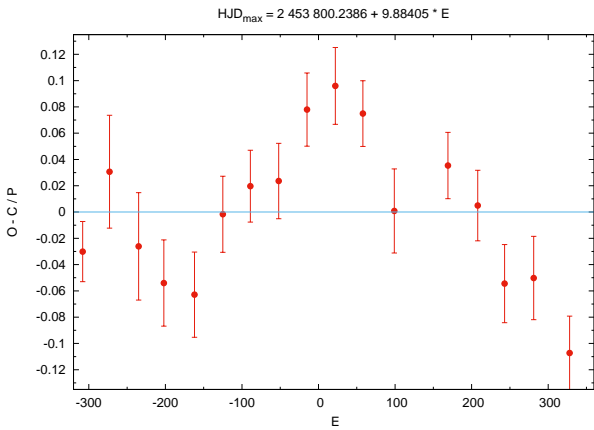


Figure 7. The observed minus calculated diagram for f_2 .

Paschen series in emission, along with OI 8446 (Fig. 8). The mean velocity for the central absorption of Paschen lines shown in Fig. 9 is $106 \pm 9 \text{ km s}^{-1}$. OI 8446 is blended with HI 8438 and this explains the large $V/R = 1.50 \pm 0.05$. We notice that the average spectrum reveals weak double emission in He I 5875, with peak separation $246 \pm 2 \text{ km s}^{-1}$ and central absorption with a minimum at 89.6 km s^{-1} . This emission is weak, with maximum intensity about 5% over the continuum. Emission is not detected in any other helium line. We measured for the NaD 1 line $EW = 0.160 \pm 0.005 \text{ \AA}$ suggesting $E(B - V) = 0.05$ according to the calibration provided by Munari & Zwitter (1997).

We notice that AzV322 might be a fast rotator, due to the broad absorption lines. However, we don't provide projected rotational velocity since the low S/N of our spectra impeded to separate adequately the contributions of the macro-turbulent velocity from the projected rotational velocity, being the former important for early B-type supergiants (Dufton et al. 2006).

The helium absorption lines in the single spectra are too noisy to provide reliable radial velocities for the Be-star photosphere. In the MIKE averaged spectrum, the average radial velocity of the helium lines of Table 6 is $96.5 \pm 17.2 \text{ km s}^{-1}$ (std), just slightly lower than the mean velocity of the H α emission lines that is about 102 km s^{-1} . We attribute the large scatter in helium velocities to (i): the quality of the data; noisy line profiles introduce artifacts in the velocity determined with Gaussian fits and (ii) the presence of non-radial pulsations related to the photometric oscillations. The situation is different for the emission lines, they have larger S/N

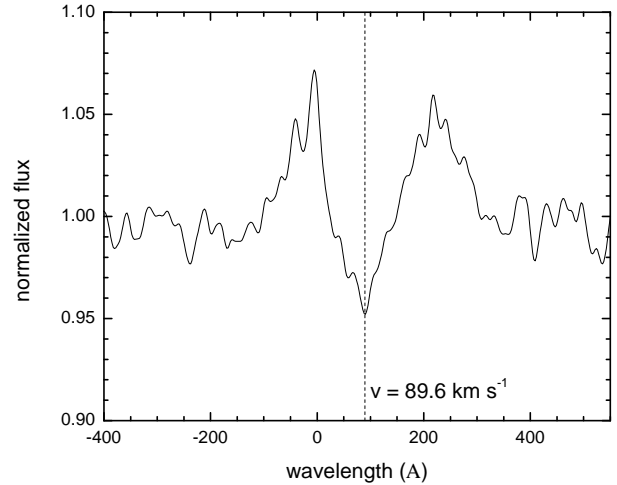
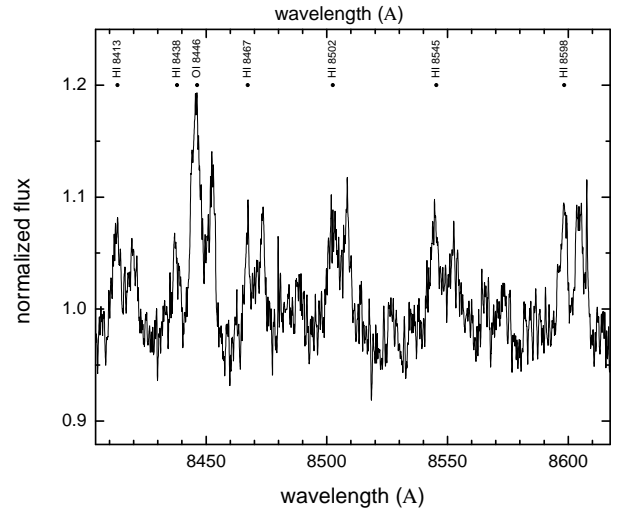
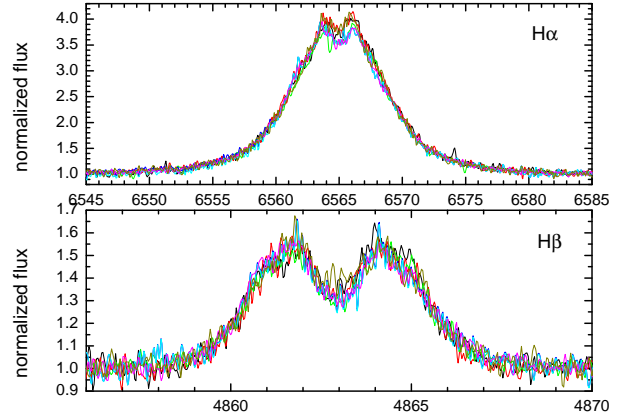


Figure 8. (Up): H α and H β profile variability for MIKE spectra. (Middle): A segment of the near-infrared spectral range in the MIKE mean spectrum. Hydrogen Paschen lines are labeled, along with OI 8446. (Down): The He I 5875 line profile in the MIKE mean spectrum.

ratio and their radial velocity errors are smaller, probably around 2 km s^{-1} , as derived from the scatter at a given epoch (Table 7).

When phasing the emission line radial velocities with the short period no relation is observed, but when phasing with the long period a smooth oscillation of amplitude about 18 km s^{-1} is observed (Fig. 9). To construct this figure we have used the ephemerides for the long-cycle with the same zero point that for the short-cycle.

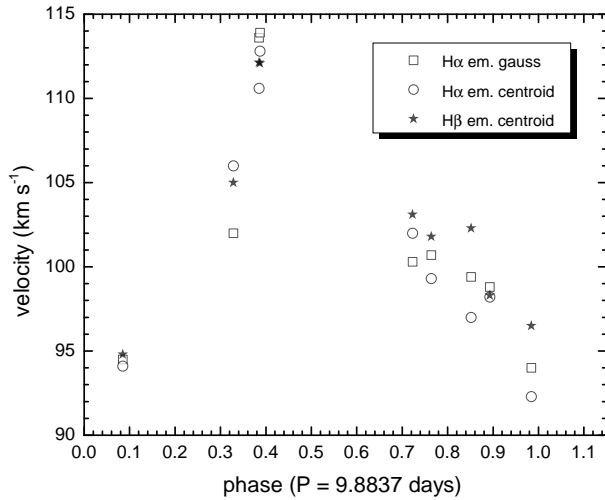


Figure 9. Radial velocities measured for different emission lines phased with the 9^d.8837 period.

Table 5. Average measurements for emission lines and their standard deviations. Data for Paschen lines shown in Fig. 8 are included, along with those for He I 5875 of the same spectrum. The fifth column gives the radius of the line forming region relative to those of He I 5875 (see text for details).

Line	EW (Å)	$\Delta\lambda$ (km s ⁻¹)	V/R	r
H α	-28.50 ± 1.10	95.1 ± 9.0	0.97 ± 0.05	6.69
H β	-2.95 ± 0.46	159.3 ± 15.3	0.99 ± 0.03	2.38
H γ	-0.47 ± 0.08	198.6 ± 5.1	0.98 ± 0.03	1.53
Paschen	-0.80 ± 0.13	227 ± 21	1.06 ± 0.27	1.17
He I 5875	-0.16 ± 0.02	246 ± 2	1.15 ± 0.05	1.00

4.3 Spectral energy distribution and stellar parameters

The spectral energy distribution was constructed by compiling the published fluxes at different bands available in the Vizier SED viewer service⁹. A Marquant-Levenberg non-linear least square fit to the observed fluxes was done with a synthetic spectrum using the formula:

$$f_{\lambda,reddened} = f_{\lambda}(R/d)^2 10^{-0.4E(B-V)[k(\lambda-V)+R(V)]}, \quad (1)$$

where f_{λ} is the stellar flux and R the stellar radius, $k(\lambda - V) \equiv$

⁹ <http://vizier.u-strasbg.fr/vizier/sed/>

Table 6. Radial velocity measured with a gaussian fit in the average spectrum.

Line	wavelength (Å)	RV (km s ⁻¹)
He I	3819	83.0 ± 1.0
He I	4009	125.4 ± 3.1
He I	4026	92.9 ± 1.0
He I	4143	107.0 ± 1.0
He I	4387	92.1 ± 1.0
He I	4922	78.5 ± 1.6
Mean	-	96.5 ± 17.2

Table 7. Radial velocities of emission lines measured with line gaussian fits or with the centroid of the emission line. The typical error, obtained from the scatter of velocities measured at a given phase, is 2 km s⁻¹.

HJD	RV_{α} (km s ⁻¹) Gauss	RV_{α} (km s ⁻¹) Centroid	RV_{β} (km s ⁻¹) Centroid
2454010.69670	102.0	106.0	105.0
2454065.69103	98.8	98.2	98.3
2454301.63094	100.7	99.3	101.8
2454412.52745	94.0	92.3	96.5
2454413.51920	94.5	94.1	94.8
2454470.51848	99.4	97.0	102.3
2454004.70866	100.3	102.0	103.1
2455068.80851	113.6	110.6	112.1
2455068.83272	113.9	112.8	112.1
Average ± std	101.9 ± 7.2	101.4 ± 7.1	102.9 ± 6.2

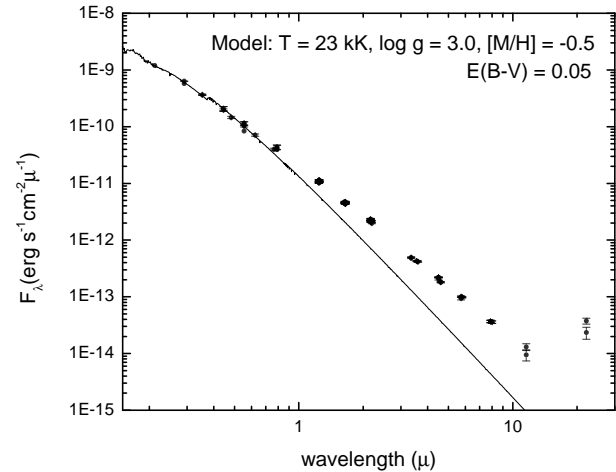


Figure 10. The spectral energy distribution and the best synthetic model.

$E(\lambda - V)/E(B - V)$ is the normalized extinction curve, $R(V) \equiv A(\lambda)/E(B - V)$ is the ratio of reddening to extinction at V and d is the distance to the system. In absence of any other better approach, we used the average Galactic Extinction Curve parametrized by Fitzpatrick & Massa (2007) to calculate reddened fluxes. We used a synthetic spectrum characterized by $T = 23$ kK, $\log g = 3.0$ and $[M/H] = -0.5$, from the grid of models given by Castelli & Kurucz (<http://wwwuser.oat.ts.astro.it/castelli/>). Models with temperatures 18, 26 and 30 kK were also tested by failed to reproduce well the SED. We adopt as the system temperature $T = 23\,000 \pm 1500$ K, that fits the effective temperature calibration for a B0.5 supergiant provided by Lefever, Puls, & Aerts (2007). The free parameters of the fit were R/d and $E(B - V)$. The best fit, minimizing χ^2 , was obtained considering fluxes with wavelengths shorter than 0.7μ . It gave $(R/d)^2 = 1.33(4)E-22$ and $E(B - V) = 0.046 \pm 0.004$ mag (Fig. 10). This exercise confirms the color excess determined from the equivalent width of the NaD 1 line and shows the evident color excess at wavelengths longer than 0.7μ . It also gives the stellar radius; considering $d = 60.6 \pm 1.0$ Kpc (Hilditch et al. 2005) we get $R = 31.0 \pm 1.1 R_{\odot}$. We notice that the longest wavelength flux, corresponding to a magnitude of a filter centered in $22 \mu\text{m}$ obtained by the Wide-field Infrared Survey Explorer (WISE) (Wright et al. 2010), is probably an artifact, since no star appears in the coordinates of the object in the corresponding WISE image.

We calculate a visual extinction of $A_V = 3.1 \times E(B - V) = 0.155 \pm 0.012$ mag. The absolute magnitude is $M_V = V - A_V + 5 - 5 \log d = -5.23 \pm 0.02$ mag, considering the average $V = 13.84$ (Table 1). Using a bolometric correction of $BC = -2.21 \pm 0.15$ for $T_{eff} = 23 \pm 1.5$ kK (Flower 1996), we get a bolometric magnitude of $M_{bol} = -7.44 \pm 0.15$ and a bolometric luminosity of $L_{bol} = 10^{4.87 \pm 0.06} L_{\odot}$.

The mass of AzV322 is $16 \pm 1 M_{\odot}$, as determined from its position in the HR diagram and the evolutionary tracks by Maeder & Meynet (2001) for rotating stars with a low metallicity of $Z = 0.002$, proper for the Small Magellanic Cloud.

In order to estimate the rotational period of the star P_{rot} (in days) we use the basic kinematics formula:

$$\frac{r}{R_{\odot}} = \frac{P_{rot} v}{50.633}, \quad (2)$$

where r is the distance to the centre of rotation and v the linear velocity of material at the equator of the star measured in km s^{-1} . Using $r = 31.0 R_{\odot}$, $i \geq 30^\circ$ and the mean projected rotational velocities for B0-B2 stars of luminosity class I in the Galaxy, viz. $69 \pm 7 \text{ km s}^{-1}$ (Abt, Levato, & Grosso 2002) we get $P_{rot} \geq 11$ days. We see that the short cycle is too small to be the rotational period of the star. Also half of the rotational period (due for instance to two stellar spots) is hard to accept due to the symmetric light curve and its stability through the years. The rotational hypothesis is also weak due to the presence of additional frequencies in the light curve.

5 DISCUSSION

5.1 The disk

The double peak emission and the Balmer progression with smaller peak separations at the lower members of the Balmer series suggest that the shape of the line emitting circumstellar envelope is disk-like (Rivinius, Carciofi, & Martayan 2013). The disk can also be responsible for the infrared excess, as usual for Be star disks, through the scattering of the stellar light by free electrons in the envelope whose visibility is proportional to the disk projected area and hence better at intermediate latitudes (Dachs et al. 1988). It is surprising that AzV322, being a B0.5 supergiant, does not show the typical emission line pattern of an outflowing radiatively driven wind, i.e. a set of P-Cygni profiles, as usually observed in these systems (Lefever, Puls, & Aerts 2007). We notice that the cause for this might be a rapid rotation, which should be able to sustain a circumstellar disk like in Classical Be stars. A disk formed by mass transfer in a close binary is other possible hypothesis, but no sign of a close binary is found, see below.

Assuming an optically thin Keplerian disk we can determine the relative velocities of the line forming regions as given in Table 5, following the relationship (Huang 1972):

$$\frac{\Delta \lambda}{2 \sin i} = \sqrt{\frac{GM}{r}}, \quad (3)$$

where $\Delta \lambda$ is the peak separation in velocity units and r the radius of the disk emitting region. We find that the $H\alpha$, $H\beta$, $H\gamma$ and Paschen disks are 6.7, 2.4, 1.5 and 1.2 times larger than the disk region forming He I 5875, respectively. Considering the stellar mass derived in Section 4.3 we determine absolute extensions for disk line emitting regions of $6.4 \sin^2 i R_{\star}$ ($202 \sin^2 i R_{\odot}$) for the He I 5875 line forming region and $42.8 \sin^2 i R_{\star}$ ($1349 \sin^2 i R_{\odot}$) for the $H\alpha$ line forming

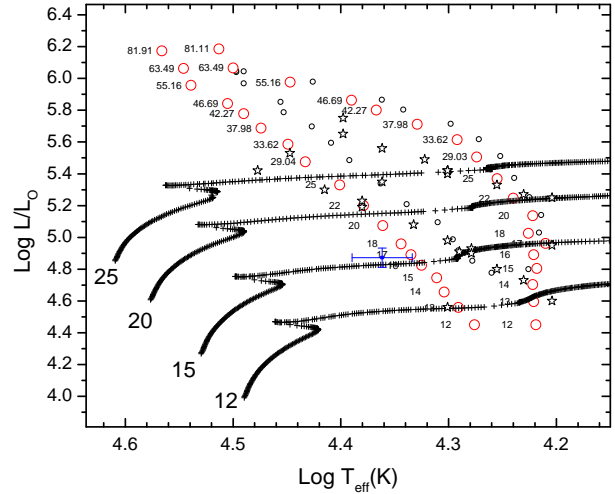


Figure 11. The position of AzV322 in the HR diagram along with the stability boundaries for $l = 1$ (small circles) and $l = 2$ (big circles) gravitationally driven models for metallicity $Z = 0.004$ of Saio et al. (2006). Some evolutionary tracks from Maeder & Meynet (2001) are also shown along with the position of periodically variable supergiants (stars) according to Lefever, Puls, & Aerts (2007). Tracks and boundaries are labeled in solar masses.

region. For intermediate latitudes (e.g. $i = 60^\circ$, $\sin^2 i = 0.75$), we obtain a $H\alpha$ disk of radius $32.1 R_{\star}$, which is larger than typical Be star $H\alpha$ disks, whose radial extension are $3\text{--}16 R_{\star}$ (Rivinius, Carciofi, & Martayan 2013). It is possible that this can be explained by the larger budget of UV photons available in the supergiant able to ionize a larger fraction of the circumstellar envelope than in classical Be stars. On the other hand, the long-term photometric variability shown in Fig. 4, of 0.1 mag amplitude in 17.5 years in the I -band, is typical for Be stars and possibly explained by electron scattering in circumstellar envelopes of variable density (Dachs & Rohe 1990).

5.2 On the short period and g-mode pulsations

As mentioned above, the main photometric period of AzV322 is shorter than the stellar rotational period, hence it cannot be described by rotation of spots or some kind of surface activity. Also, as said before, the rotational hypothesis cannot explain the presence of multiple photometric frequencies. On the contrary, the stability of the periodicities through the years (apart from the variability for f_1 timings discussed below) suggests an explanation in terms of stellar pulsations as we show in this section.

AzV322 fits well the luminosity- T_{eff} plane of periodically variable B-type supergiants (Fig. 11). These have been interpreted in terms of non-radial gravity-mode oscillations (Saio et al. 2006; Lefever, Puls, & Aerts 2007; Ostrowski & Daszyńska-Daszkiewicz 2015) and this can be a possible interpretation for the periodicities found in AzV322.

The main and secondary photometric periods of AzV322 and their amplitudes fit well the parameters of other B-type supergiants showing periodically variable oscillations (Fig. 12). This finding strengthens even more the interpretation of the photometric periodicity in terms of g-mode pulsations.

We notice that the observed changes in times of maximum observed in the O-C diagram for the frequency f_1 might be interpreted in terms of a light-travel time effect in a wide-orbit binary. This effect was first suggested for the Algol system by Chandler (1888)

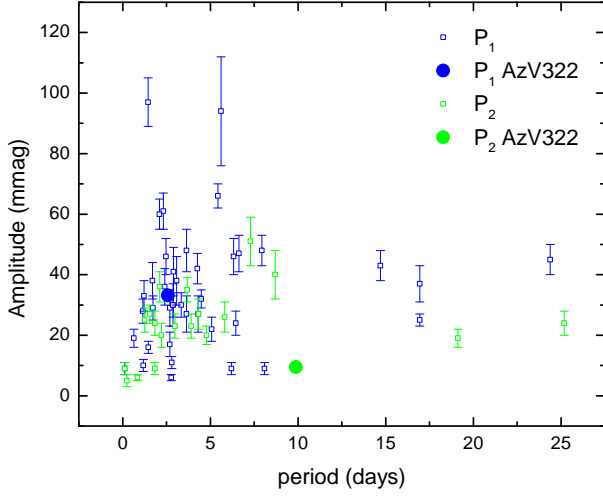


Figure 12. Comparison with the periodically variable B-type supergiants of Lefever, Puls, & Aerts (2007). Main and secondary periods and their amplitudes are shown.

and theoretical tools for its analysis were developed by Woltjer (1922) and Irwin (1952). It has been noticed that the solution of the inverse problem in which the best solution is determined still remains a problem (Liška et al. 2016). It is beyond the hope of this paper to inquire on the solution of this particular phenomenon since a detailed analysis should require data distributed on several decades. It is enough to say here that if the variability is due to the light-travel time effect, it should indicate a very wide-orbit and long-period binary. The differences in phase of the order of 0.1 cycles for f_1 imply time differences of about 0.25 days implying a light travel path of $6.475E9$ km i.e. $9308 R_{\odot}$, or in terms of the stellar radius $295R_{\star}$. This should correspond to the projected semi-major axis of the barycentric orbit of the B-type star, about 9 times the extension derived for the $H\alpha$ emitting disk.

5.3 Does the long period reflect a binary motion?

The fact that the centroid of the $H\alpha$ emission line varies with the long periodicity (f_2) suggests that it could represent the period of a binary star in an elliptical orbit. The $H\alpha$ is relatively strong and we can easily determine its radial velocity at every epoch, which is harder for the weak and noisy photospheric Helium lines. Actually, helium line RVs show an erratic pattern when phased with f_2 .

Let's investigate if the $H\alpha$ radial velocities can be represented by the orbital motion of a binary. We use the genetic algorithm PIKAIA (Charbonneau 1995) to determine the orbital parameters that best fit the available data. Following the analysis described by Mennickent et al. (2012, 2015) we minimize χ^2 defined as:

$$\chi^2(P, \tau, \omega, e, K, \gamma) = \frac{1}{N-6} \sum_{j=1}^n \left(\frac{V_j - V(t_j, P, \tau, \omega, e, K, \gamma)}{\sigma_j} \right)^2, \quad (4)$$

where N is the number of observations, V_j and V the observed and calculated velocities in time t_j . The theoretical velocity is:

$$V(t) = \gamma + K((\omega + \theta(t)) + e \cos(\omega)), \quad (5)$$

where θ is the true anomaly obtained by solving the equations:

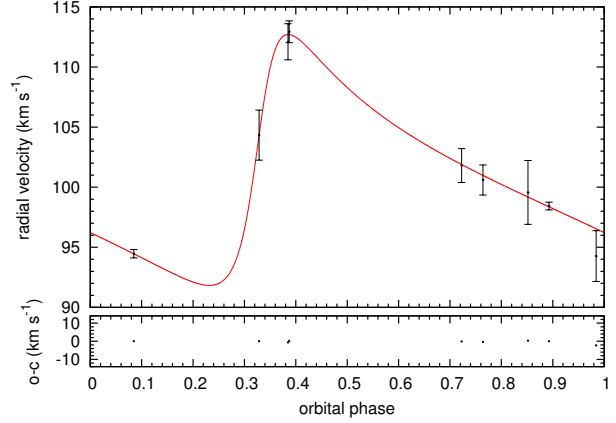


Figure 13. Averaged radial velocities per phase and the best orbital fit.

Table 8. Orbital elements for the donor of AzV322 obtained by minimization of the χ^2 parameter given by Eq. 4. The value $\tau^* = \tau - 2450000$ and the limits of the confidence intervals within one standard deviation (1σ) are given.

Parameter	Best value	Lower limit	Upper limit
P_o (d)	9.88370 (fixed)		
τ^*	4010.71631	4010.71802	4020.55615
ω (rad)	4.96994	4.91379	5.03079
e	0.59115	0.54371	0.63985
K_2 (km s $^{-1}$)	10.44027	10.07962	11.02156
γ (km s $^{-1}$)	100.69585	100.42592	100.98771
χ^2		0.51479	

$$\tan\left(\frac{\theta}{2}\right) = \sqrt{\frac{1+e}{1-e}} \tan\left(\frac{E}{2}\right), \quad (6)$$

$$E - e \sin(E) = \frac{2\pi}{P}(t - \tau), \quad (7)$$

where E is the eccentric anomaly. We fixed the period, constrained the eccentricity between 0 and 1, ω between 0 and 2π , τ between the minimum HJD and this value plus the period, K between 0 and $(V_{max} - V_{min})$ and γ between V_{min} and V_{max} .

In order to estimate the errors for the results obtained from PIKAIA, we proceeded to calculate the confidence intervals for the region corresponding to 68.26% of the sample (1σ) through a routine created in PYTHON for this purpose. The results are given in Table 8. Our results reveal a very eccentric orbit ($e = 0.655$) and the fit produces a good match to the available data (residuals ≈ 1 km s $^{-1}$, Fig. 13). From the results above and using the formula:

$$a \sin i = (1.9758 \times 10^{-2})(1 - e^2)^{1/2} K P R_{\odot}, \quad (8)$$

where the period P is in days and the half-amplitude of radial velocity K in kilometers per second (e.g. Hilditch 2001) we get $a_1 \sin i = 1.64 R_{\odot}$. This is a very short distance; even considering a conservative value for the inclination angle of 30° , we get $a = 3.29 R_{\odot}$. Considering that the B star is a supergiant with radius $\sim 30 R_{\odot}$, it is impossible to fit the orbit. We conclude that the radial velocity variability does not reflect a binary orbit.

Since the binary hypothesis has been rejected, other phenomenon produces the modulation of the emission lines radial velocities. The number of data points is low and more epochs are desirable to define the shape of the radial velocity (RV) curve since it

is still possible that the observed variability is product of stochastic phenomena and the low number statistics.

Looking at the Fig. 12, it is clear that the period of ν^18837 (f_2) fits the period-amplitude distribution of periodically variable B-type supergiants, so it could be a second mode of gravitationally driven pulsation.

The origin of the circumstellar envelope at present is unknown, it could be due to: (i) an unseen companion transferring mass onto the B-type star due to Roche lobe overflow or (ii) a mechanism related to g-mode pulsation, in a similar way that seems to be happening in Be stars. At present, the data is not enough to discriminate between these competent scenarios. In particular, more epochs and higher S/N spectra are needed to check the presence of a companion.

6 CONCLUSIONS

Based on the study of 17.5 years of *I* and *V*-band OGLE photometry, high-resolution optical spectra covering 8 epochs, and published photometric magnitudes from the ultraviolet to the infrared region we find that:

- AzV322 is an early B-type periodically variable supergiant surrounded by a circumstellar disk.
- Our study confirms the main photometric periodicity of 2^d587000 found by Kourniotis et al. (2014).
- The star shows additionally three significant photometric periods: ν^18837 , 2^d0503 and 1^d1438. Both the main photometric periodicity as well as these three additional frequencies can be attributed to g-mode pulsations. This conjecture is supported by the position of the star in the HR diagram very close to the recently discovered Slowly Pulsating B-type Supergiants by Saio et al. (2006) and also for the location of the star in the period-amplitude diagram.
- The star is characterized by double emission lines and infrared excess consistent with the presence of a circumstellar disk. If optically thin, this disk has extensions $7.6 \sin^2 i R_*$ for the He I 5875 line forming region and $50.8 \sin^2 i R_*$ for the H α forming region.
- The data are compatible with the following stellar parameters: $T_{eff} = 23000 \pm 1500$ K, $\log g = 3.0 \pm 0.5$, $M = 16 \pm 1 M_{\odot}$, $R = 31.0 \pm 1 R_{\odot}$, and $L_{bol} = 10^{4.87 \pm 0.06} L_{\odot}$.
- The origin of the disk is unknown, it could be related to the presence of g-mode non-radial pulsations, as happens in Be stars, or alternatively, it could be the result of mass transfer from a Roche lobe filling undetected secondary star.
- Times of maximum for the f_1 frequency vary quasi-cyclically in a time scale of 20 years. This might be interpreted as a light-travel time effect in a wide orbit binary whose secondary stellar component has not been detected.

7 ACKNOWLEDGMENTS

Thanks to the anonymous referee for providing useful comments that improved the first version of this manuscript. We thanks Dr. Hideyuki Saio for providing the theoretical data shown in Fig. 11. This publication makes use of VOSA, developed under the Spanish Virtual Observatory project supported from the Spanish MICINN through grant AyA2008-02156. This research has made use of the SIMBAD database, operated at CDS, Strasbourg, France. R.E.M. acknowledges support by VRID-Enlace 216.016.002-1.0 and the BASAL Centro de Astrofísica y Tecnologías Afines (CATA) PFB-06/2007. HEG gratefully acknowledges the financial support by

CNPq No. PDJ-152237/2016-0. The OGLE project has received funding from the Polish National Science Centre grant MAESTRO no. 2014/14/A/ST9/00121. Thanks to Maja Vuckovic, Monika Jurkovic and Angelica Jara for useful conversations during the first stages of the preparation of this manuscript.

REFERENCES

- Abt H. A., Levato H. & Grosso M. 2002, ApJ, 573, 359
 Azzopardi M., Vigneau J. & Macquet M. 1975, A&AS, 22, 285
 Baade D. et al. 2016, arXiv, arXiv:1611.01113, to appear in Proc. 2nd BRITE-Constellation Science Conference: 'small satellites - big science', Innsbruck, Aug. 2016, eds.: G. Stachowski, E. Poretti, and J. Matthews
 Chandler S. C. 1888, AJ, 7, 165
 Charbonneau P. 1995, ApJS, 101, 309
 Dachs J. 1970, A&A, 9, 95
 Dachs J. & Rohe C. 1990, A&A, 230, 380
 Dachs J., Kiehling R. & Engels D. 1988, A&A, 194, 167
 Dufton P. L. et al. 2006, A&A, 451, 603
 Flower P. J. 1996, ApJ, 469, 355
 Henize K. G. 1956, ApJS, 2, 315
 Hilditch R. W., Howarth I. D. & Harries T. J. 2005, MNRAS, 357, 304
 Huang S.-S. 1972, ApJ, 171, 549
 Irwin J. B. 1952, ApJ, 116, 211
 Kourniotis M. et al. 2014, A&A, 562, A125
 Lefever K., Puls J. & Aerts C. 2007, A&A, 463, 1093
 Lenz P. & Breger M. 2005, CoAst, 146, 53
 Liška J. et al. 2016, A&A, 589, A94
 Maeder A. & Meynet G. 2001, A&A, 373, 555
 Meyssonnier N. & Azzopardi M. 1993, A&AS, 102, 451
 Mennickent R. E. 2017, SerAJ, 194, 1
 Mennickent R. E. et al. 2003, A&A, 399, L47
 Mennickent R. E. et al. 2015, MNRAS, 448, 1137
 Mennickent R. E. et al. 2012, MNRAS, 427, 607
 Mennickent R. E., Otero S. & Kołaczowski Z. 2016, MNRAS, 455, 1728
 Ostrowski J. & Daszyńska-Daszkiewicz J. 2015, MNRAS, 447, 2378
 Rivinius T., Carciofi A. C. & Martayan C. 2013, A&ARv, 21, 69
 Saio H. et al. 2006, ApJ, 650, 1111
 Smith Neubig M. M. & Bruhweiler F. C. 1997, AJ, 114, 1951
 Szymanski M. K. 2005, AcA, 55, 43
 Tody D. 1993, ASPC, 52, 173
 Udalski A., Szymański M. K. & Szymański G. 2015, AcA, 65, 1
 Woltjer J., Jr. 1922, BAN, 1, 93
 Wright E. L. et al. 2010, AJ, 140, 1868-1881

This paper has been typeset from a $\text{\TeX}/\text{\LaTeX}$ file prepared by the author.